

Exceptional van Hove singularities in pseudogapped metals

 Indranil Paul¹ and Marcello Civelli²
¹Université Paris Cité, CNRS, Laboratoire Matériaux et Phénomènes Quantiques, 75205 Paris, France

²Université Paris-Saclay, CNRS, Laboratoire de Physique des Solides, 91405 Orsay, France

 (Received 19 October 2022; revised 9 May 2023; accepted 11 May 2023; published 30 May 2023)

Motivated by the pseudogap state of the cuprates, we introduce the concept of an “exceptional” van Hove singularity that appears when a strong electron-electron interaction splits an otherwise simply connected Fermi surface into multiply connected pieces. The singularity describes the touching of two pieces of the split Fermi surface. We show that this singularity is proximate to a second-order van Hove singularity, which can be accessed by tuning a dispersion parameter. We argue that, in a wide class of cuprates, the endpoint of the pseudogap is accessed only by triggering the exceptional van Hove singularity. The resulting Lifshitz transition is characterized by enhanced specific heat and nematic susceptibility, as seen in experiments.

 DOI: [10.1103/PhysRevB.107.L201121](https://doi.org/10.1103/PhysRevB.107.L201121)

Introduction. In electronic systems on a lattice, the periodicity of the potential guarantees the existence of saddle points of the dispersion $\epsilon_{\mathbf{k}}$ as a function of the wave vector \mathbf{k} where the velocity $\mathbf{v}_{\mathbf{k}} \equiv \nabla_{\mathbf{k}}\epsilon_{\mathbf{k}}$ vanishes [1,2]. In two dimensions such van Hove singularities give rise to a diverging density of states, which has attracted attention since the early days of condensed matter physics. Since an electron-electron interaction is not needed to produce such singularities, they are typically associated with noninteracting physics. The purpose of the current Letter is to study “exceptional” van Hove singularities, which are saddle points generated by a strong electron-electron interaction. As we show below, such a study is particularly useful to understand some unusual properties of several hole-doped cuprates close to the doping where the pseudogap disappears [3–15].

Our main observation is the following. Consider a one-band system whose Fermi surface is simply connected in the weakly interacting limit. Then, the saddle points are necessarily located at the high-symmetry points in the Brillouin zone where the Fermi surface can open or close. A typical example is the $(\pm\pi, 0)$ and $(0, \pm\pi)$ points for a square lattice when the band extremum is at $(0, 0)$ or (π, π) . This situation is to be contrasted with the case where the interaction is strong enough to induce self-energy corrections that are singular, such as in a pseudogap phase. Then, as shown in Figs. 1(a)–1(c), the self-energy splits the simply connected Fermi surface into a multiply connected surface (i.e., Fermi pockets, or annular Fermi surfaces), and the saddle point is a result of the touching of two pieces of that surface. In this case the saddle points are not located on the high-symmetry points, but they lie on the high-symmetry lines [see arrows in Fig. 1(b)], which has important consequences. We describe the resulting interaction-driven van Hove singularity as being “exceptional,” to distinguish it from ordinary van Hove singularities that are obtained in the weakly interacting limit.

Model. The canonical system to illustrate the physics of exceptional van Hove singularities is certain underdoped cuprates in the pseudogap state. Motivated by the Yang-Rice-Zhang (YRZ) model [16], we describe it by a single band of

electrons whose Green’s function is given by

$$G_{\mathbf{k}}(i\omega_n)^{-1} = i\omega_n - \epsilon_{\mathbf{k}} - P_{\mathbf{k}}^2/(i\omega_n - \xi_{\mathbf{k}}). \quad (1)$$

This type of model has been justified through phenomenological [16–20] as well as numerical [21–30] cluster dynamical mean-field studies of the strong-coupling Hubbard model.

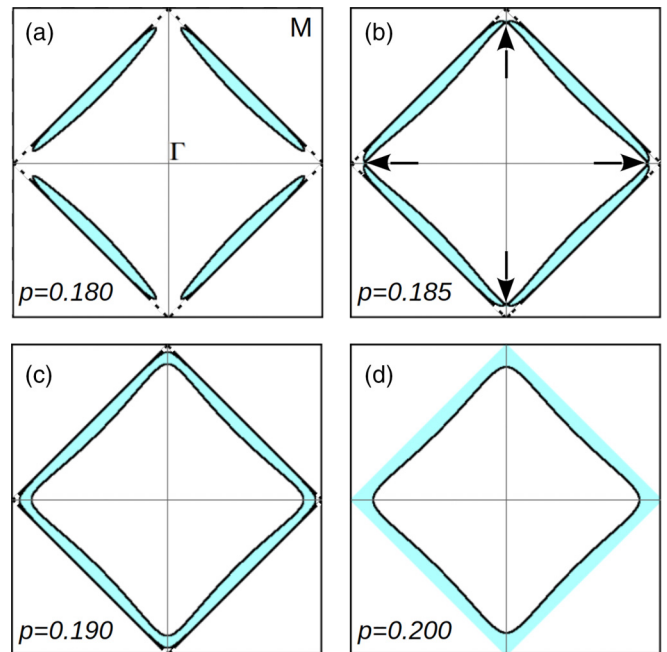


FIG. 1. Fermi-surface evolution with doping near the pseudogap endpoint. Hole occupation is indicated by the blue shade. (a) Singular self-energy splits a simply connected Fermi surface into hole pockets. (b) The hole pockets enlarge with doping, and they touch at exceptional van Hove points (indicated by arrows), located on the high-symmetry lines, but not on the high-symmetry points. (c) Further doping forms annular rings of holes. (d) When the pseudogap vanishes, a closed electronlike weakly interacting Fermi surface is recovered.

An extensive comparison with experiments using the YRZ model has also been reported in Ref. [31]. Here, $\epsilon_{\mathbf{k}} = -2\tilde{t}(\cos k_x + \cos k_y) - 4t'\cos k_x \cos k_y - \mu$ is the electron dispersion, $\tilde{t}(p) = t[1 - 4(0.2 - p)]$ is a hopping parameter modified by the interaction, $t = 1$, $t' = -0.15$, p is the hole doping, and μ is the chemical potential. We take $\xi_{\mathbf{k}} = 2\tilde{t}(\cos k_x + \cos k_y)$, where the equation $\xi_{\mathbf{k}} = -\omega$ defines the points on the Brillouin zone where the electron's spectral weight is suppressed due to the pseudogap. We model the pseudogap by $P_{\mathbf{k}}(p) = \theta(p^* - p)P_0(1 - p/p^*)(\cos k_x - \cos k_y)$, where $\theta(x)$ is the Heaviside step function, $P_0 = 0.4$ is the pseudogap energy at half filling ($p = 0$), and which decreases linearly with hole doping, and terminates at $p^* = 0.2$. All energy scales are in units of t , which we take to be about 300 meV [32] for later estimates.

Superficially, Eq. (1) is reminiscent of two hybridizing bands, namely the physical electrons with dispersion $\epsilon_{\mathbf{k}}$ and pseudofermions with dispersion $\xi_{\mathbf{k}}$. Thus, it can be written as

$$G_{\mathbf{k}}(i\omega_n) = A_{1\mathbf{k}}/(i\omega_n - \omega_{1\mathbf{k}}) + A_{2\mathbf{k}}/(i\omega_n - \omega_{2\mathbf{k}}), \quad (2)$$

where $\omega_{1\mathbf{k},2\mathbf{k}} = [\epsilon_{\mathbf{k}} + \xi_{\mathbf{k}} \pm \sqrt{(\epsilon_{\mathbf{k}} - \xi_{\mathbf{k}})^2 + 4P_{\mathbf{k}}^2}]/2$. The weight factors $A_{1\mathbf{k}} = (\omega_{1\mathbf{k}} - \xi_{\mathbf{k}})/(\omega_{1\mathbf{k}} - \omega_{2\mathbf{k}})$, and $A_{2\mathbf{k}} = (\xi_{\mathbf{k}} - \omega_{2\mathbf{k}})/(\omega_{1\mathbf{k}} - \omega_{2\mathbf{k}})$. For the doping range studied here only the lower band $\omega_{2\mathbf{k}}$ contributes to the Fermi surface in the form of hole pockets that evolves with doping [see Fig. 1 and Fig. S4 in the Supplemental Material (SM) [33]].

Exceptional van Hove singularity. As shown in Fig. 1, with increasing doping the hole pockets grow and eventually, at a doping $p_{ev} \approx 0.185$, the pockets touch at the van Hove points $(0, \pm k_{ev})$ and $(\pm k_{ev}, 0)$, where $k_{ev} \neq \pi$ [see arrows in Fig. 1(b)]. The resulting Lifshitz transition describes hole pockets merging to form hole rings [see Fig. 1(c)].

In the vicinity of such saddle points, say, the one at $(0, k_{ev})$, the dispersion can be expressed as $\omega_{2\mathbf{k}} \approx \alpha k_x^2 - \beta k_y^2 - \gamma k_y k_x^2$, where (α, β, γ) are parameters with dimension of energy, and $\gamma \neq 0$ indicates that the saddle point is not on a high-symmetry location. The peak in the density of states $\rho(\omega) \equiv -(1/\pi) \sum_{\mathbf{k}} \text{Im} G_{\mathbf{k}}(\omega + i\Gamma)$ near the singularity is given by $\rho(\omega) \approx 4\rho_{sp}(\omega)$, where

$$\rho_{sp}(\omega) = \frac{1}{2\pi^2 \sqrt{\alpha\beta}} \left[\text{Re} \left[\frac{1}{(1+u)^{1/4}} K(r_1) \right] - \text{Im} \left[\frac{1}{(1+u)^{1/4}} K(r_2) \right] \right]. \quad (3)$$

Here, $u = (\omega + i\Gamma)/E_0$, $E_0 = \alpha^2 \beta / \gamma^2$, $r_{1,2} = [1 \pm 1/(1+u)^{1/2}]/2$, and $K(r) \equiv \int_0^{\pi/2} d\theta / \sqrt{1 - r^2 \sin^2 \theta}$ is the complete elliptic integral of the first kind, and $\Gamma = 0.01t$ is a frequency-independent inverse lifetime.

In Fig. 2 we show the evolution of the peak in the density of states with doping. As $p \rightarrow p_{ev}$, the peak position moves from negative energies $\omega < 0$, and approaches the chemical potential $\omega = 0$. However, for the cuprates, increasing doping also implies a reduction in the pseudogap strength $P_{\mathbf{k}}(p)$. Therefore, the strength of the singularity decreases upon approaching the Lifshitz transition. This is seen as the diminishing peak height of $\rho(\omega)$ with doping in Fig. 2.

Proximity to second-order van Hove singularity. This is a consequence of $\gamma \neq 0$. In Fig. 3(a) we plot the curvature

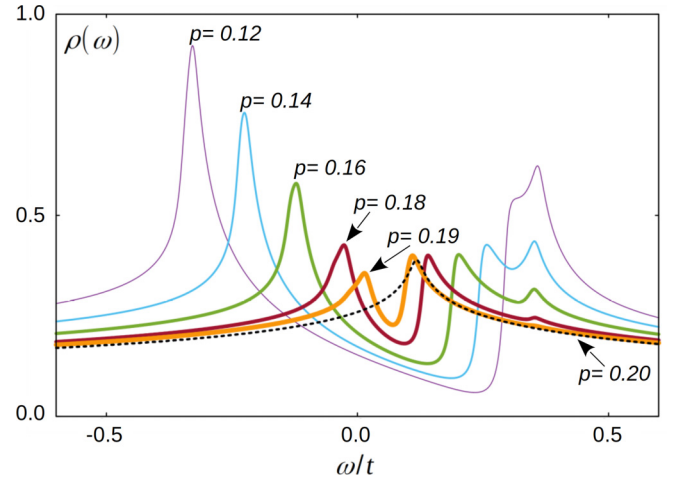


FIG. 2. Density of states $\rho(\omega)$ for various dopings. The exceptional van Hove singularity manifests as a peak which is at negative energies ω for low doping. The peak height diminishes as the pseudogap potential decreases with doping. The peak crosses $\omega = 0$ at $p_{ev} \approx 0.185$.

$\alpha_{\mathbf{k}} \equiv \partial^2 \omega_{2\mathbf{k}} / \partial k_x^2$ along the $(0, 0)$ - $(0, \pi)$ direction for various dopings. We notice that, when the pseudogap is sufficiently small ($p \geq 0.16$), $\alpha_{(0,k_y)}$ has positive values at $k_y \sim 0$, and it has negative values at $k_y \sim \pi$, implying it goes through zero at $k_y = k_2 \sim \alpha/\gamma$.

If $\alpha_{\mathbf{k}} = 0$ and $\mathbf{v}_{\mathbf{k}} = 0$ are simultaneously satisfied, the system has a second-order van Hove singularity [37–42]. The density of states has a power-law singularity, obtained by taking $\alpha \rightarrow 0$ in Eq. (3), instead of the usual log singularity. In our case these two points are located close by on the same high-symmetry lines, i.e., $k_{ev} \sim k_2$, implying that the system is close to the second-order singularity, and therefore the prefactor of the log is large. Indeed, we find that as $p \rightarrow p^*$, the wave vectors k_{ev} and k_2 come closer, as shown in Fig. 3(b). As shown in Figs. S1 and S2 of the SM [33], the conversion to second-order singularity can be readily achieved by varying a third-nearest-neighbor hopping parameter which, *a priori*, is feasible in cold atom systems.

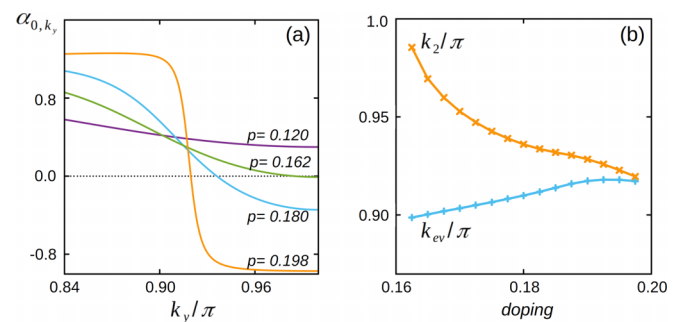


FIG. 3. (a) Plot of $\alpha_{\mathbf{k}} \equiv \partial^2 \omega_{2\mathbf{k}} / \partial k_x^2$ along the $(0, 0)$ - $(0, \pi)$ direction for various dopings. For $p > 0.162$ in the current model, the curvature $\alpha_{\mathbf{k}}$ vanishes at $(0, k_2)$ and symmetry equivalent points. (b) Variation of k_2 and k_{ev} with doping. Near the pseudogap endpoint the exceptional van Hove singularity is close to a second-order one, and the prefactor of the log in the density of states is large.

Note, for a single-band system with a simply connected Fermi surface, no such proximity to a second-order van Hove singularity is expected. Thus, in such systems, this proximity distinguishes an interaction-induced exceptional van Hove singularity from a weakly interacting ordinary one. In multi-band systems, however, higher-order van Hove singularities can arise from noninteracting physics alone [37–42].

Exceptional van Hove singularity near pseudogap endpoint. In the rest of this Letter we examine the relevance of exceptional van Hove singularities for the cuprates in the vicinity of the hole doping p^* where the pseudogap terminates.

First, we explain why, for a large class of cuprates, the chemical potential necessarily crosses the exceptional van Hove singularity as the pseudogap endpoint is approached from the underdoped side. As a function of doping (or equivalently the chemical potential) the evolution of the Fermi surface can be tracked by solving the equation $\text{Re}[G_{\mathbf{k}}(\omega = 0)^{-1}] = 0$. In the absence of any pseudogap term, the self-energy corrections are analytic, and therefore the Fermi surface is bound to cross the $(0, \pi)$ and $(\pi, 0)$ points at a doping p_0 where the ordinary (or the weakly interacting) van Hove singularity crosses the chemical potential, thereby transforming from an open to a closed Fermi surface of electrons. In the presence of the pseudogap, however, at $\omega = 0$ the Fermi surface cannot cross these points since the pseudogap term is a divergent repulsive potential on the manifold $\xi_{\mathbf{k}} = 0$ where these points lie. Generally, there are three possible ways in which the Fermi-surface evolution can respond to this divergence.

The first is the possibility that the pseudogap terminates at a doping exactly where the chemical potential crosses the ordinary van Hove singularity, i.e., $p^* = p_0$. In this case the open Fermi surface can close smoothly by crossing the $(0, \pi)$ and $(\pi, 0)$ points. However, this will occur only if the system is fine tuned. Since such a coincidence is unlikely in general, we do not discuss it further.

The second possibility is that the pseudogap terminates before the ordinary van Hove singularity is reached, i.e., $p^* < p_0$. In this case, for the doping range $p_0 > p > p^*$, the pseudogap term is zero, the self-energy is analytic, and therefore the open Fermi surface can close smoothly by crossing the $(0, \pi)$ and $(\pi, 0)$ points. A recent study has shown that this is indeed the case for cuprates for which $|t'/t|$ is sufficiently large, such as $\text{YBa}_2\text{Cu}_3\text{O}_{7-\delta}$ (YBCO), $\text{Tl}_2\text{Ba}_2\text{CuO}_{6+\delta}$, and $\text{HgBa}_2\text{CuO}_{4+\delta}$ [27].

The third possibility, namely $p^* > p_0$, triggers the exceptional van Hove singularity studied here. It is relevant for cuprates for which $|t'/t|$ is sufficiently small, such as $\text{Bi}_2\text{Sr}_2\text{CaCu}_2\text{O}_{8+\delta}$, $(\text{Bi}, \text{Pb})_2(\text{Sr}, \text{La})_2\text{CuO}_{6+\delta}$, $\text{La}_{2-x}\text{Sr}_x\text{CuO}_4$ (LSCO), and (Nd, Eu)-LSCO [27]. In this case, the hole pockets grow with increasing hole doping, but simultaneously the Fermi surface avoids the $(0, \pi)$ and $(\pi, 0)$ points, since $P_{\mathbf{k}} \neq 0$. In such a situation there is invariably a doping p_{ev} , with $p^* > p_{ev} > p_0$, for which the chemical potential crosses the exceptional van Hove singularity and the hole pockets touch at points which lie on the high-symmetry lines such as $(0, 0) - (0, \pi)$ [see Fig. 1(b)]. Beyond the Lifshitz transition, for $p^* > p > p_{ev}$, the hole pockets merge into

a ring of holes with annular Fermi surfaces [see Fig. 1(c)]. Then, as $p \rightarrow p^*$, the inner Fermi surface of the hole ring merges with $\epsilon_{\mathbf{k}} = 0$ and the outer Fermi surface of the hole ring merges with the line of Luttinger zeros $\xi_{\mathbf{k}} = 0$ [see Fig. 1(d)].

Therefore, we predict that, in the narrow doping range $p_{ev} < p < p^*$ separating the Lifshitz transition from the pseudogap endpoint, the holes form an annular ring bounded by two Fermi surfaces [see Fig. 1(c)], with the physical electron weight mostly on the inner Fermi surface. From an angle-resolved photoemission perspective this is a state with a closed Fermi surface, but where the $(\pi, 0)$ point is still pseudogapped. Note, this narrow doping range may be difficult to resolve in an experiment. In that case it will appear that the Lifshitz transition and the closing of the pseudogap occur at the same doping, as reported in the recent literature [6–8, 27, 28].

Experimental signatures. Recently, signatures of unusual thermodynamics have been reported for several cuprates close to the pseudogap endpoint p^* . Thus, the specific-heat coefficients $\gamma(T)$ of LSCO, (Nd, Eu)-LSCO, Ca-doped YBCO, and $\text{Bi}_{2+y}\text{Sr}_{2-x-y}\text{La}_x\text{CuO}_{6+\delta}$ show a logarithmic T dependence [4, 15], while the nematic susceptibility $\chi_{B_{1g}}$ of $\text{Bi}_2\text{Sr}_2\text{CaCu}_2\text{O}_{8+\delta}$ increases considerably in this doping range [5, 6]. Both these observations can be potentially explained by the presence of a nematic quantum critical point (QCP) around p^* , but no such QCP has been identified until now. Moreover, even though an ordinary van Hove singularity can lead to $\gamma(T) \sim \log T$, the observed anomaly was deemed too sharp for such an explanation [4, 15]. As we show below, the above experimental puzzles can be resolved if we assume the presence of an exceptional van Hove singularity, i.e., these systems follow the third possibility discussed above.

We compute the specific-heat coefficient $\gamma(T) = C(T)/T$ using

$$C(T) = \int_{-\infty}^{\infty} d\omega \frac{\omega^2/T^2}{\cosh^2[\omega/(2T)]} \rho(\omega),$$

and we show its (p, T) evolution in Fig. 4. As $p \rightarrow p_{ev}$, there is a distinct upturn in the T dependence of the specific-heat coefficient, reminiscent of what has been reported for in Refs. [4, 15] with $\gamma(T) \sim \log T$. In our computation there is indeed such a logarithmic component. However, the overall T dependence in our theory is way more complex, just as is the frequency dependence of the density of states in Eq. (3).

The p dependence of $\gamma(T \rightarrow 0, p)$ is also similar to what has been reported in Refs. [4, 15]. As shown in the inset of Fig. 4, it has sharp maxima around $p = p_{ev}$, which is close to but not coincident with p^* . This sharp feature can be contrasted with the weak-coupling case by setting the pseudogap term $P_{\mathbf{k}} = 0$. As shown by the red dotted line in the inset of Fig. 4, the peak is broader and far less pronounced for an ordinary van Hove singularity compared to an exceptional one. This is because the latter is close to a second-order van Hove instability. Also, the bands are flatter than usual for the exceptional case since the velocity vanishes at two proximate points $(0, k_{ev})$ and $(0, \pi)$, instead of only at $(0, \pi)$.

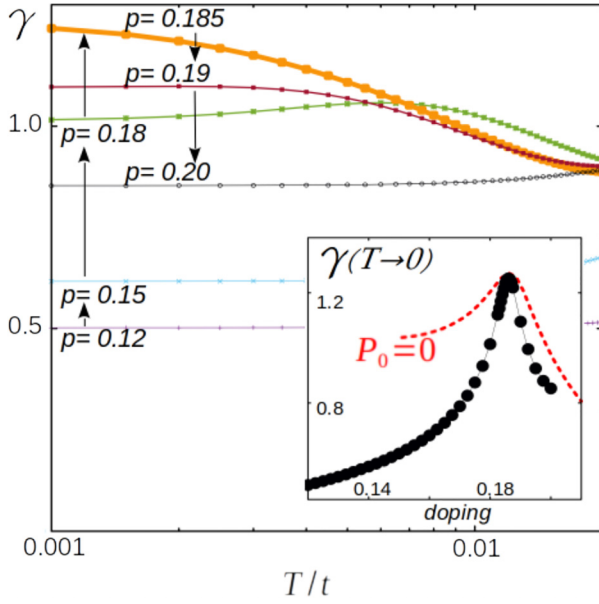


FIG. 4. Specific-heat coefficient γ as a function of temperature and doping. Arrows indicate that γ increases as $p \rightarrow p_{ev}$, where the exceptional van Hove singularity is on the chemical potential. At $p = p_{ev}$, the saturation of $\gamma(T)$ with temperature is pushed to lower T . The inset shows the doping dependence of $\gamma(T \rightarrow 0)$ (black dots) with a sharp peak at $p = p_{ev}$. The red dotted line is the calculation for an ordinary van Hove singularity obtained for pseudogap $P_k = 0$, and shifted horizontally and vertically for better comparison. The peak is sharper and more pronounced for an exceptional van Hove singularity.

Next, we study the nematic susceptibility in the B_{1g} or the $(x^2 - y^2)$ symmetry channel, which is given by

$$\chi_{B_{1g}} = -\text{Im} \left[\sum_{\mathbf{k}} h_{\mathbf{k}, B_{1g}}^2 \int_{-\infty}^{\infty} \frac{d\omega}{2\pi} \tanh\left(\frac{\omega}{2T}\right) G_{\mathbf{k}}(\omega + i\Gamma)^2 \right],$$

with $h_{\mathbf{k}, B_{1g}} = \partial^2 \epsilon_{\mathbf{k}} / \partial k_x^2 - \partial^2 \epsilon_{\mathbf{k}} / \partial k_y^2$. In Fig. 5 we present the (p, T) dependencies of $\chi_{B_{1g}}^{-1}$. It has weak T dependence away from the critical doping p_{ev} , while at p_{ev} it decreases considerably with lowering temperature [equivalently, $\chi_{B_{1g}}(T)$ increases with lowering T], which can be fitted to a Curie-Weiss behavior above a temperature cutoff. Taking $t \sim 300$ meV, the temperature range of the Curie-Weiss behavior in our calculation is 100–300 K, which matches well with the range seen in the experiments. Thus, our result is qualitatively close to what has been reported for $\text{Bi}_2\text{Sr}_2\text{CaCu}_2\text{O}_{8+\delta}$ in Fig. 2(b) of Ref. [5]. Note, the low-temperature downturn in $\chi_{B_{1g}}^{-1}$ for $p \sim p_{ev}$ seen in Fig. 5 is a theoretical prediction that can be checked by performing Raman spectroscopy at lower temperatures. Finally, the inset of Fig. 5 shows the doping dependence of $T_0 \equiv \chi_{B_{1g}}^{-1}(T = 0)$. Once again, the nonmonotonic p dependence, with T_0 coming close to zero (equivalently, large $\chi_{B_{1g}}$) around $p \sim p_{ev}$, captures what is reported in Fig. 3 of Ref. [5].

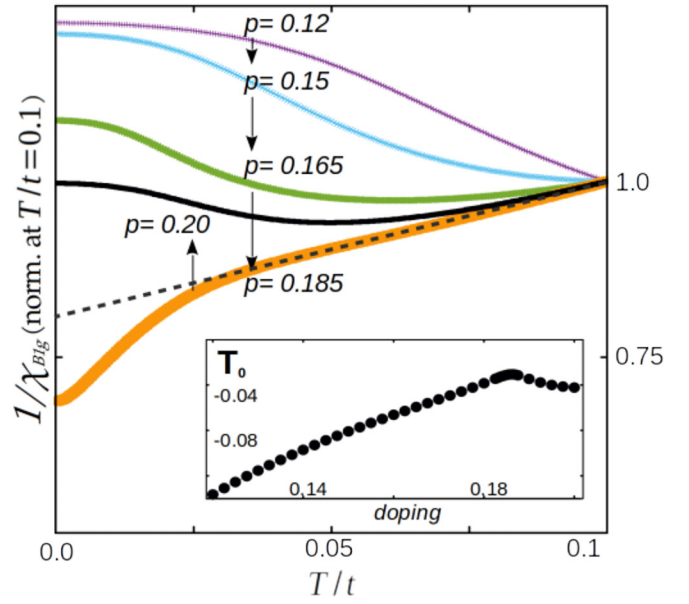


FIG. 5. Temperature and doping dependence of the inverse nematic susceptibility $\chi_{B_{1g}}^{-1}$ in the $(x^2 - y^2)$ channel. The T dependence enhances considerably around p_{ev} , with Curie-Weiss $1/T$ scaling above a cutoff temperature (black dashed line). The inset shows the doping dependence of $T_0 \equiv \chi_{B_{1g}}^{-1}(T \rightarrow 0)$ with a peak near p_{ev} .

Conclusion. In summary, motivated by the pseudogap state of the cuprates, we introduced the concept of a strong interaction-driven “exceptional” van Hove singularity. It appears when the single-particle dispersion has a singular correction that splits an otherwise simply connected Fermi surface into multiply connected pieces. The exceptional van Hove singularity describes the touching of two pieces of the split Fermi surface. The associated saddle points of the renormalized dispersion are located, not on the high-symmetry points, but on the high-symmetry lines of the Brillouin zone. This feature is proximate to a second-order van Hove singularity. Consequently, the logarithmic divergence of the density of states is guaranteed to have a large prefactor. Most importantly, we argued that several hole-doped cuprates necessarily encounter an exceptional van Hove point as they approach the pseudogap endpoint, and we showed that the signatures of the singularity can explain recent experiments [4–6,15]. We expect the electronic dispersion to show features of the exceptional van Hove which can be detected by photoemission [43,44] (see the discussion associated with Figs. S3–S5 of the SM for further details [33]).

Finally, our work can be extended in two directions in the future: first, to study interaction-driven second van Hove singularities, and second, to study exceptional van Hove singularities in heavy fermions, where the Kondo coupling with the localized spins provides a singular correction to the conduction electron dispersion.

Acknowledgments. We are thankful to M. C. O. Aguiar, Y. Gallais, F. Piéchon, A. Sacuto, and L. Taillefer for insightful discussions. We acknowledge financial support from French Agence Nationale de la Recherche (ANR) Grant No. ANR-19-CE30-0019-01 (Neptun).

- [1] L. van Hove, *Phys. Rev.* **89**, 1189 (1953).
- [2] See, e.g., N. W. Ashcroft and N. D. Mermin, *Solid State Physics* (Saunders College Publishing, Philadelphia, 1976), Chap. 8.
- [3] For reviews, see, e.g., C. Proust and L. Taillefer, *Annu. Rev. Condens. Matter Phys.* **10**, 409 (2019); I. M. Vishik, *Rep. Prog. Phys.* **81**, 062501 (2018); M. R. Norman and C. Pépin, *ibid.* **66**, 1547 (2003).
- [4] B. Michon, C. Girod, S. Badoux, J. Kačmarčík, Q. Ma, M. Dragomir, H. A. Dabkowska, B. D. Gaulin, J.-S. Zhou, S. Pyon, T. Takayama, H. Takagi, S. Verret, N. Doiron-Leyraud, C. Marcenat, L. Taillefer, and T. Klein, *Nature (London)* **567**, 218 (2019).
- [5] N. Auvray, S. Benhabib, M. Cazayous, R. D. Zhong, J. Schneeloch, G. D. Gu, A. Forget, D. Colson, I. Paul, A. Sacuto, and Y. Gallais, *Nat. Commun.* **10**, 5209 (2019).
- [6] S. Benhabib, A. Sacuto, M. Civelli, I. Paul, M. Cazayous, Y. Gallais, M.-A. Méasson, R. D. Zhong, J. Schneeloch, G. D. Gu, D. Colson, and A. Forget, *Phys. Rev. Lett.* **114**, 147001 (2015).
- [7] B. Loret, S. Sakai, S. Benhabib, Y. Gallais, M. Cazayous, M. A. Méasson, R. D. Zhong, J. Schneeloch, G. D. Gu, A. Forget, D. Colson, I. Paul, M. Civelli, and A. Sacuto, *Phys. Rev. B* **96**, 094525 (2017).
- [8] N. Doiron-Leyraud, O. Cyr-Choinière, S. Badoux, A. Ataei, C. Collignon, A. Gourgout, S. Dufour-Beausejour, F. F. Tafti, F. Laliberté, M. Matusiak, D. Graf, M. Kim, J.-S. Zhou, N. Momono, T. Kurosawa, H. Takagi, and L. Taillefer, *Nat. Commun.* **8**, 2044 (2017).
- [9] C. Collignon, A. Ataei, A. Gourgout, S. Badoux, M. Lizaire, A. Legros, S. Licciardello, S. Wiedmann, J.-Q. Yan, J.-S. Zhou, Q. Ma, B. D. Gaulin, N. Doiron-Leyraud, and L. Taillefer, *Phys. Rev. B* **103**, 155102 (2021).
- [10] B. Michon, A. B. Kuzmenko, M. K. Tran, B. McElfresh, S. Komiya, S. Ono, S. Uchida, and D. van der Marel, *Phys. Rev. Res.* **3**, 043125 (2021).
- [11] Y. Fang, G. Grissonnanche, A. Legros, S. Verret, F. Laliberté, C. Collignon, A. Ataei, M. Dion, J. Zhou, D. Graf, M. J. Lawler, P. Goddard, L. Taillefer, and B. J. Ramshaw, *Nat. Phys.* **18**, 558 (2022).
- [12] A. Gourgout, G. Grissonnanche, F. Laliberté, A. Ataei, L. Chen, S. Verret, J.-S. Zhou, J. Mravlje, A. Georges, N. Doiron-Leyraud, and L. Taillefer, *Phys. Rev. X* **12**, 011037 (2022).
- [13] M. Zhu, D. J. Voneshen, S. Raymond, O. J. Lipscombe, C. C. Tam, and S. M. Hayden, *Nat. Phys.* **19**, 99 (2023).
- [14] J. Küspert, R. Cohn Wagner, C. Lin, K. von Arx, Q. Wang, K. Kramer, W. R. Pudalko, N. C. Plumb, C. E. Matt, C. G. Fatuzzo, D. Sutter, Y. Sassa, J.-Q. Yan, J.-S. Zhou, J. B. Goodenough, S. Pyon, T. Takayama, H. Takagi, T. Kurosawa, N. Momono, M. Oda *et al.*, [arXiv:2207.07424](https://arxiv.org/abs/2207.07424).
- [15] C. Girod, D. LeBoeuf, A. Demuer, G. Seyfarth, S. Imajo, K. Kindo, Y. Kohama, M. Lizaire, A. Legros, A. Gourgout, H. Takagi, T. Kurosawa, M. Oda, N. Momono, J. Chang, S. Ono, G.-q. Zheng, C. Marcenat, L. Taillefer, and T. Klein, *Phys. Rev. B* **103**, 214506 (2021).
- [16] K.-Y. Yang, T. M. Rice, and F.-C. Zhang, *Phys. Rev. B* **73**, 174501 (2006).
- [17] M. R. Norman, M. Randeria, H. Ding, and J. C. Campuzano, *Phys. Rev. B* **57**, R11093(R) (1998).
- [18] M. R. Norman, A. Kanigel, M. Randeria, U. Chatterjee, and J. C. Campuzano, *Phys. Rev. B* **76**, 174501 (2007).
- [19] E. Bascones and B. Valenzuela, *Phys. Rev. B* **77**, 024527 (2008).
- [20] J. G. Storey, *Europhys. Lett.* **113**, 27003 (2016).
- [21] B. Kyung, S. S. Kancharla, D. Sénéchal, A.-M. S. Tremblay, M. Civelli, and G. Kotliar, *Phys. Rev. B* **73**, 165114 (2006).
- [22] T. D. Stanescu and G. Kotliar, *Phys. Rev. B* **74**, 125110 (2006).
- [23] A. Liebsch and N.-H. Tong, *Phys. Rev. B* **80**, 165126 (2009).
- [24] M. Civelli, *Phys. Rev. B* **79**, 195113 (2009).
- [25] S. Sakai, Y. Motome, and M. Imada, *Phys. Rev. Lett.* **102**, 056404 (2009).
- [26] S. Sakai, M. Civelli, and M. Imada, *Phys. Rev. Lett.* **116**, 057003 (2016).
- [27] W. Wu, M. S. Scheurer, S. Chatterjee, S. Sachdev, A. Georges, and M. Ferrero, *Phys. Rev. X* **8**, 021048 (2018).
- [28] H. Bragança, S. Sakai, M. C. O. Aguiar, and M. Civelli, *Phys. Rev. Lett.* **120**, 067002 (2018).
- [29] G. Sordi, K. Haule, and A.-M. S. Tremblay, *Phys. Rev. Lett.* **104**, 226402 (2010).
- [30] G. Sordi, K. Haule, and A.-M. S. Tremblay, *Phys. Rev. B* **84**, 075161 (2011).
- [31] T. M. Rice, K.-Y. Yang, and F. C. Zhang, *Rep. Prog. Phys.* **75**, 016502 (2012).
- [32] O. K. Andersen, A. I. Liechtenstein, O. Jepsen, and F. Paulsen, *J. Phys. Chem. Solids* **56**, 1573 (1995).
- [33] See Supplemental Material at <http://link.aps.org/supplemental/10.1103/PhysRevB.107.L201121> for further details, which includes Refs. [34–36].
- [34] A. Damascelli, Z. Hussain, and Z.-X. Shen, *Rev. Mod. Phys.* **75**, 473 (2003).
- [35] H.-B. Yang, J. D. Rameau, P. D. Johnson, T. Valla, A. Tsvetlik, and G. D. Gu, *Nature (London)* **456**, 77 (2008).
- [36] M. Zonno, F. Boschini, and A. Damascelli, *J. Electron Spectrosc. Relat. Phenom.* **251**, 147091 (2021).
- [37] A. Tamai, M. P. Allan, J. F. Mercure, W. Meevasana, R. Dunkel, D. H. Lu, R. S. Perry, A. P. Mackenzie, D. J. Singh, Z.-X. Shen, and F. Baumberger, *Phys. Rev. Lett.* **101**, 026407 (2008).
- [38] A. Shtyk, G. Goldstein, and C. Chamon, *Phys. Rev. B* **95**, 035137 (2017).
- [39] D. V. Efremov, A. Shtyk, A. W. Rost, C. Chamon, A. P. Mackenzie, and J. J. Betouras, *Phys. Rev. Lett.* **123**, 207202 (2019).
- [40] N. F. Q. Yuan, H. Isobe, and L. Fu, *Nat. Commun.* **10**, 5769 (2019).
- [41] Y.-T. Hsu, F. Wu, and S. D. Sarma, *Phys. Rev. B* **104**, 195134 (2021).
- [42] D. Guerci, P. Simon, and C. Mora, *Phys. Rev. Res.* **4**, L012013 (2022).
- [43] B. Loret, Y. Gallais, M. Cazayous, R. D. Zhong, J. Schneeloch, G. D. Gu, A. Fedorov, T. K. Kim, S. V. Borisenko, and A. Sacuto, *Phys. Rev. B* **97**, 174521 (2018).
- [44] Y. Zhong, Z. Chen, S.-D. Chen, K.-J. Xu, M. Hashimoto, Y. He, S.-i. Uchida, D. Lu, S.-K. Mo, and Z.-X. Shen, *Proc. Natl. Acad. Sci. USA* **119**, e2204630119 (2022).